INSTITUTE OF PHYSICS PUBLISHING and INTERNATIONAL ATOMIC ENERGY AGENCY NUCLEAR FUSION

Nucl. Fusion **43** (2003) 1632–1640 PII: S0029-5515(03)69604-3

Overview of the FTU results

B. Angelini, M.L. Apicella, G. Apruzzese, E. Barbato, A. Bertocchi, G. Bracco, A. Bruschi[1], G. Buceti, P. Buratti, A. Cardinali, L. Carraro[2], C. Castaldo, C. Centioli, R. Cesario, S. Cirant[1], V. Cocilovo, F. Crisanti, R. De Angelis, M. De Benedetti, G. Giruzzi[3], F. De Marco, B. Esposito, M. Finkenthal[4], D. Frigione, L. Gabellieri, F. Gandini[1], L. Garzotti[2], G. Gatti, E. Giovannozzi, C. Gormezano, F. Gravanti, G. Granucci[1], M. Grolli, F. Iannone, H. Kroegler, E. Lazzaro[1], M. Leigheb, G. Maddaluno, G. Maffia, M. Marinucci, M. Mattioli[5], G. Mazzitelli, F. Mirizzi, S. Nowak[1], D. Pacella, L. Panaccione, M. Panella, P. Papitto, V. Pericoli-Ridolfini, A.A. Petrov[6], L. Pieroni, S. Podda, F. Poli[5], M.E. Puiatti[2], G. Ravera, G.B. Righetti, F. Romanelli, M. Romanelli, F. Santini, M. Sassi, A. Saviliev[7], P. Scarin[2], S.E. Segre[8], A. Simonetto[1], P. Smeulders, E. Sternini, C. Sozzi[1], N. Tartoni, B. Tilia, A.A. Tuccillo, O. Tudisco, M. Valisa[2], V. Vershkov[9], V. Vitale, G. Vlad, V. Zanza, M. Zerbini and F. Zonca

Associazione EURATOM-ENEA sulla Fusione CR Frascati, 00044, Frascati, Roma, Italy
[1] Associazione EURATOM-ENEA-CNR sulla Fusione, Istituto di Fisica del Plasma, Milano, Italy
[2] Consorzio RFX, Corso Stati Uniti 4, I-35100, Padova, Italy
[3] Association EURATOM-CEA, Cadarache, F-13108, Saint-Paul-lez-Durance, France
[4] The Johns Hopkins University, Baltimore, MD21218, USA
[5] ENEA guest
[6] State Research Center of Russian Federation, Troitsk Institute for Innovation and Fusion Research, SRC RF TRINITI, Troitsk, Moscow region, 142190, Russia
[7] AF Ioffe Physico-Technical Institute RAS, Polytechnicheskaya 26, 194021 St Petersburg, Russian Federation
[8] Dipartimento di Fisica, II Università di Roma 'Tor Vergata', Roma Italy
[9] Nuclear Fusion Institute, RRC Kurchatov Institute, 123182, Kurchatov Sq. 1, Moscow, Russian Federation

E-mail: romanelli@frascati.enea.it

Received 15 October 2002, accepted for publication 16 September 2003
Published 1 December 2003
Online at stacks.iop.org/NF/43/1632

Abstract
An overview of the Frascati tokamak upgrade (FTU) results during the period 2000–2002 is presented. Long duration internal transport barriers (ITBs) have been obtained on FTU with combined injection of lower hybrid (LH) and electron cyclotron (EC) waves in 5 T/0.5 MA discharges. The ITB phase lasts about 10 energy confinement times and is characterized by an energy confinement time up to 1.6 times the ITER97 L-mode scaling. Temperatures up to 11 keV are measured at 0.9×10^{20} m^{-3} central density. ITB studies using IBW injection have also been continued up to 8 T/0.8 MA. The LH system has operated at full power allowing us to complete the current drive (CD) studies at ITER-relevant densities. At these density values the electrons and ions are coupled and an increase in the ion temperature is clearly observed. A preliminary sign of enhanced CD efficiency has been obtained in the combined injection of EC and LH waves at magnetic field values lower than the resonant field for thermal EC absorption. Pellet optimization studies have been performed in order to test the conditions under which a quasi-steady-state confinement improvement can be obtained and impurity accumulation can be avoided. The confinement time in Ohmic discharges is generally in agreement with the ITER97 L-mode scaling. Transient confinement improvement is observed for a duration less than one energy confinement time. Radiation improved mode studies have been started thanks to the recently inserted boronization system, which has allowed reduction of the radiated power. Confinement improvement with neon injection has been observed in 6 T/0.9 MA discharges. Transport studies on profile stiffness and magnetohydrodynamic (MHD) studies of fast reconnection and snakes will also be presented.

PACS numbers: 52.55.Fa, 52.50.Sw

1. Introduction

The Frascati tokamak upgrade (FTU) ($a = 0.3$ m, $R = 0.93$ m) is a compact, high magnetic field tokamak aimed at studying confinement, stability and wave–particle interaction physics at ITER-relevant parameters by operating up to a magnetic field of $B = 8$ T and a plasma current of $I = 1.6$ MA. The main upgrades with respect to the last IAEA conference have been the insertion of a boronization system and of a second ion Bernstein wave (IBW) antenna. The boronization system has allowed us to achieve very clean plasmas and to reduce the radiated power fraction down to a level as low as 30%, allowing, in particular, radiation improved (RI) mode studies to be started. During the last two years most of the effort has been focused on the investigation of internal transport barriers (ITBs) with electron heating at high density, i.e. close to reactor-relevant conditions. This has been obtained by the combined injection of lower hybrid (LH) waves, to control the current density profile, and electron cyclotron (EC) waves, to produce large electron temperature gradients. Long-lasting ITBs can now be routinely produced in the FTU with a duration of the order of several confinement times, limited by the duration of the ECRH phase. These discharges exhibit an enhancement of the global energy confinement time over the ITER97 L-mode scaling up to a factor 1.6, in contrast with typical Ohmic and L-mode discharges that follow such a scaling. Pellet enhanced performance (PEP) discharges, characterized by very high neutron rates, exhibit transient confinement improved phases, lasting less than one energy confinement time, up to a factor 1.3 above the ITER97 scaling. Pellet optimization studies have shown that in order to avoid high-Z impurity accumulation (the FTU is equipped with a TZM toroidal limiter) in the presence of peaked density profiles, delayed sawteeth must be maintained. This allows a long sequence of PEP mode phases with quasi-steady-state H factors well above those achieved in gas fuelled discharges.

The FTU is equipped with three different RF heating systems that have been extensively used for the production and control of ITBs. The LH system (8 GHz, $t_{\mathrm{pulse}} = 1$ s) is composed of six gyrotrons feeding six grills on two FTU windows. The system has operated close to the maximum performance ($\approx$2 MW at the plasma). The EC resonance heating (ECRH) system [1] (140 GHz, $t_{\mathrm{pulse}} = 0.5$ s) has been working at a maximum power level of about 0.8 MW at the plasma (corresponding to two gyrotrons), making use of the launching system capability of injecting power at an oblique angle with current drive (CD) capability. The system has been employed both for transport studies and magnetohydrodynamic (MHD) mode stabilization. Synergy studies with combined injection of LH and EC waves have been made in the ITER-relevant upshifted scheme. Encouraging preliminary results with the IBW system at higher power have been obtained.

2. ITB studies

2.1. Long duration ITBs with combined LHCD and ECRH

ITBs have been observed in the past in the FTU using ECRH on the current ramp in $B = 5.3$ T discharges [2]. Very high values of the central electron temperature ($\approx$15 keV) were observed with the electron thermal conductivity maintaining the value of the Ohmic phase, in spite of much larger temperature and temperature gradients. These discharges were characterized by a large value of the radiated power (this was, in fact, used to produce hollow temperature and current density profiles in the early phase of the discharge) due to heavy impurity contamination. In order to avoid such a problem, scenarios have been developed with simultaneous injection of LH and EC waves both during the current ramp and the current flat top. As in most of the existing experiments, ECRH injection during the current ramp phase delays the current density evolution and allows the formation of broad current density profiles that are subsequently maintained by LHCD during the flat top phase [3]. In this way, long-lasting electron ITBs have been obtained [4]. As shown in figure 1(*a*), the duration of the ITB phase is of the order of 0.25 s corresponding to about 10 energy confinement times, with the central density reaching 0.9×10^{20} m^{-3} and the central temperature up to about 11 keV as confirmed by spectroscopic measurements of heavy-impurity line radiation. After the ECRH phase, the ITB becomes weaker and then disappears possibly due to a change in the current density profile or an increase of the plasma collisionality. In order to achieve steady-state conditions, a different ITB formation scheme has been attempted. A plasma target is formed with full LHCD. The EC power is applied during the flat top phase in order to produce an electron ITB (figure 1(*b*)). Again, the ITB duration is limited by the duration of the ECRH phase.

Transport analysis has been carried out for the discharge shown in figure 1(*a*) using the JETTO code [5]. The LH power deposition and CD profiles are calculated by one-dimensional Fokker–Planck Bonoli code [3]. The ECRH power deposition is calculated by a ray-tracing code. The transport analysis shows a reduction of the electron thermal diffusivity, more pronounced in the time interval 0.24–0.34 s. The code shows the formation of a negative magnetic shear configuration. From the radial T_{e} profile (figure 1(*c*)), an expansion of the ITB is observed, which might be correlated to a broadening of the LH power deposition profile observed in the simulation (figure 1(*d*)). An improvement of the ion confinement is observed in the time range 0.24–0.34 s. The ion thermal diffusivity χ_{i} in FTU can be often modelled by an anomaly factor of the neoclassical diffusivity ($\chi_{\mathrm{i}} = A \times \chi_{\mathrm{Chang–Hinton}}$, with A the anomaly factor and the neoclassical thermal diffusivity given by the Chang–Hinton expression). The time evolution of the experimental neutron rate and the experimental ion temperature on axis can be modelled, by reducing the anomaly factor by 60%. It is important to stress that plasma density peaking is also observed during this ITB phase. The ITB degradation is followed by the onset of MHD $m = 1$, $m = 2$ coupled modes (at $t = 0.34$ s).

As shown in figure 1(*e*), a transition occurs from pure L-mode scaling to improved confinement when ρ^* ($\rho^* = \rho_{\mathrm{i}}/L_{\mathrm{T}}$, ρ_{i} being the ion sound Larmor radius and L_{T} the temperature scale length) exceeds a threshold value similar to the value observed in JET for obtaining an ITB [6]. The global energy confinement time shows an enhancement up to a factor of 1.6 times the ITER97 L-mode scaling. The maximum ρ^* value over the plasma minor radius is used.

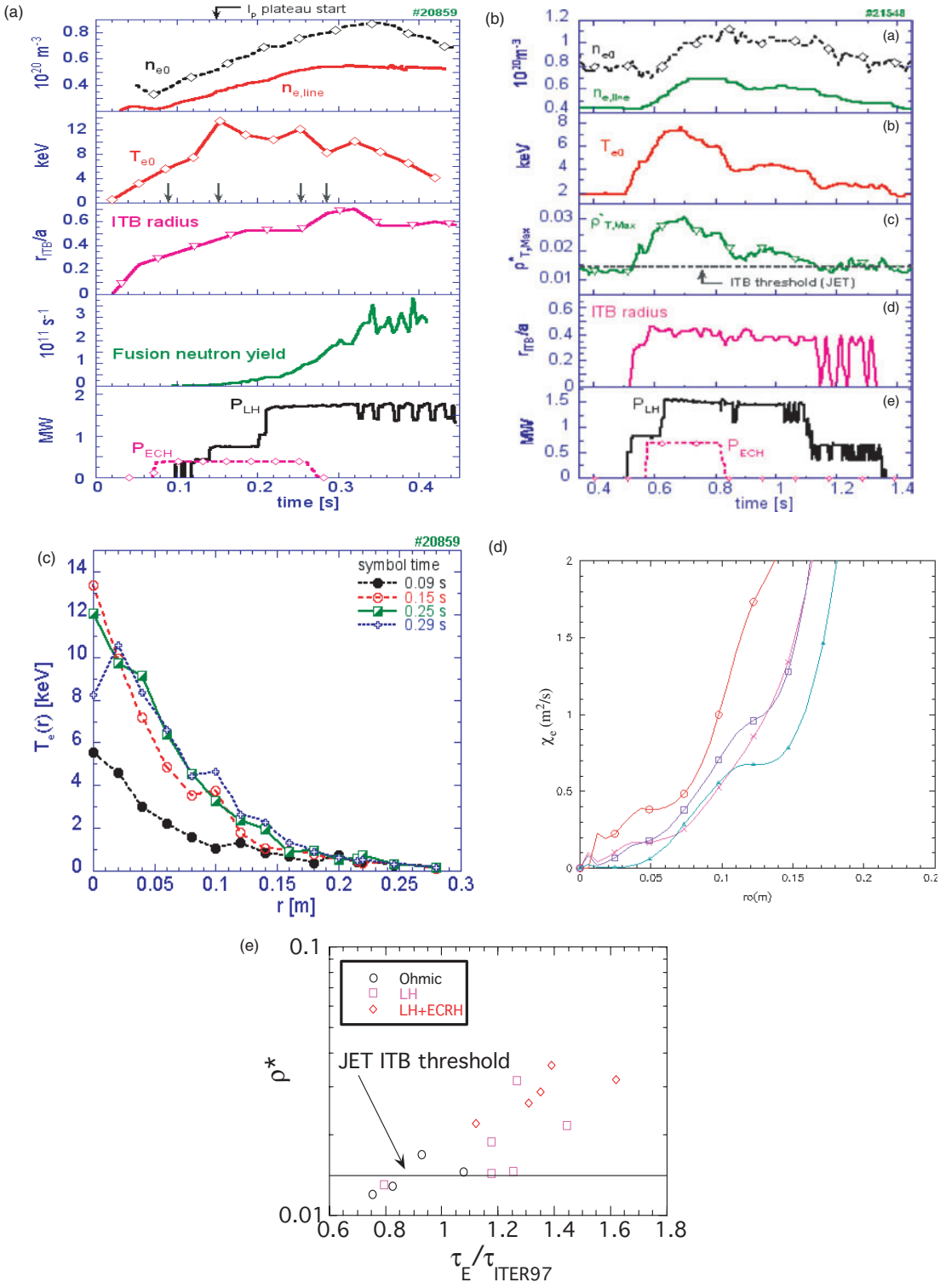

Figure 1. (*a*) Time evolution of central (n_{e0}) and line average ($n_{e,line}$) density, central electron temperature (T_{e0}), normalized ITB radius, neutron yield and LH (P_{LH}) and EC (P_{ECH}) power for the discharge #20859 with an ITB obtained by ECRH during the current ramp-up and LHCD in the flat-top to maintain a broad current profile. The time at which the current plateau starts is also shown. The arrows indicate four different time slices at which the temperature profile is shown in (*c*). (*b*) Time evolution of central (n_{e0}) and line average ($n_{e,line}$) density, central electron temperature (T_{e0}), maximum normalized ion sound Larmor radius ($\rho^*_{T,Max}$), normalized ITB radius, LH (P_{LH}) and EC (P_{ECH}) power for the discharge #21548 with the ITB obtained by ECRH during the current flat-top on a target discharge with full LHCD. (*c*) Time evolution of the electron temperature profiles for the discharge shown in (*a*). The various times correspond to the arrows in (*a*). (*d*) Radial profile of the electron thermal conductivity for the four profiles shown in (*c*). The expansion of the ITB radius with time is apparent. (*e*) ρ^* vs $\tau_E/\tau_{ITER\ 97\text{-}th}$: the maximum of ρ^* over the plasma minor radius is used. The threshold value found on JET for achieving ITBs is also shown.

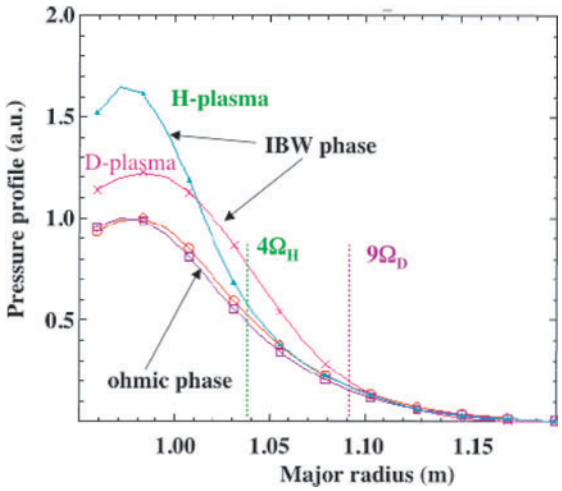

Figure 2. Pressure profile before (Ohmic phase) and after IBW injection in D and H discharges at 0.4 MA/7.9 T. The location of the absorption radius is also shown.

2.2. ITBs produced by IBW induced sheared flows

The investigation of ITB formation by IBW injection has continued with higher power capability, after the insertion of a second IBW launcher, using higher density, higher plasma current and lower $Z_{\rm eff}$ values than in the 1999 campaign [7]. In H plasmas, the IBW absorption layer is located at about one-third of the minor radius (at $4\,\Omega_{\rm H}$); the investigation has been carried out with plasma current/magnetic field values up to 0.4 MA/7.9 T and simultaneous density and temperature peaking has been observed, as during the 1999 campaign (figure 2). Deuterium plasmas have also been investigated up to 0.8 MA/7.9 T. In these conditions the absorption layer is located at a larger normalized radius ($r_{\rm abs}/a \approx 0.65$). The experimental results for a D discharge (figure 2) seems to indicate a larger ITB radius, in agreement with the position of the absorption layer (at $9\,\Omega_{\rm D}$). During the IBW injection an increase of plasma density is observed, at constant electron temperature, together with a decrease of $Z_{\rm eff}$. Thermal transport analysis shows a uniform 20% decrease of the electron thermal conductivity for the region $r < r_{\rm abs}$.

3. Radiofrequency heating studies

3.1. LHCD at high density

The FTU LHCD experiment was originally designed in order to demonstrate the feasibility of LHCD at ITER-relevant densities. During the last two years it has been possible to operate the LH system at close to full power. Conditions of full CD have been achieved at higher density, higher plasma current and lower $Z_{\rm eff}$ than before. An example of a plasma discharge close to full power for about 1 s is shown in figure 3(*a*) [8, 9].

Following the first tests of the boronization system, the decrease of the radiated power produced an increase of the heat loads on the stainless steel protection structures of the fast MHD measurements inside the vacuum chamber. The resulting increase of the temperature of the protection structures produced a large Mn evaporation followed by a disruption. During the 2001 winter campaign all the protection structures were dismantled and this problem was eliminated.

An example of a full LHCD discharge with $I = 0.50$ MA and $B = 7.2$ T is shown in figure 3(*b*). The launched $n_{||}$ spectrum has a maximum at $n_{||} = 1.52$. The peak and average density are $1.3 \times 10^{20}\,{\rm m}^{-3}$ and $0.75 \times 10^{20}\,{\rm m}^{-3}$, respectively. The electron temperature increases from 2 keV in the Ohmic phase to 6.0–4.5 keV in the auxiliary heated phase. At these density values the electron–ion coupling is large and ion heating is deduced from the large increase of the neutron rate. The neutron yield increases by a factor 6 indicating an ion temperature increase of 0.25 keV. A relatively low impurity content is maintained in these conditions: $Z_{\rm eff}$ increases from $Z_{\rm eff} = 1.7$ during the Ohmic phase to $Z_{\rm eff} = 2.7$ during the LH phase. Note that at higher densities $Z_{\rm eff}$ remains below 2 during the LH phase. The CD efficiency achieved in these discharges is $\eta_{\rm CD} = 0.23 \times 10^{20}\,{\rm A\,W^{-1}\,m^{-2}}$ and taking in account the $Z_{\rm eff}$ correction reaches the value of $\eta_{\rm CD} = 0.28 \times 10^{20}\,{\rm A\,W^{-1}\,m^{-2}}$. The LHCD efficiencies observed in the FTU show a clear dependence on the average electron temperature $\langle T_{\rm e}\rangle$ when the correction for the impurity content is accounted for [10]. In figure 3(*c*), the value of the LHCD efficiency extrapolated to $Z_{\rm eff} = 1$ is plotted vs $\langle T_{\rm e}\rangle$ for various devices showing that values in the range $\eta_{\rm CD} = 0.3 \times 10^{20}\,{\rm A\,W^{-1}\,m^{-2}}$ are achieved in a domain relevant to ITER.

3.2. Synergy studies in combined injection of LH and EC waves

Synergistic effects between LH and EC radiofrequency waves open the possibility of combining the most interesting features of the two heating schemes, namely a high CD efficiency for LH waves and a very localized, tuneable, and effective heating for EC waves. The FTU is equipped with both LH and EC systems and can perform such an investigation at ITER-relevant density values. Clear macroscopic effects were reported at the last IAEA Conference: a substantial temperature increase was obtained with $P_{\rm LH}$ up to 0.9 MW, $P_{\rm EC}$ up to 0.75 MW, $B = 7.2$ T (cold EC resonance outside the vacuum vessel) and central plasma density up to $0.7 \times 10^{20}\,{\rm m}^{-3}$ in the reported domain of studies [11]. The synergy LHCD–EC is characterized by a substantial damping of the EC wave on the energetic LHCD-produced electrons at a magnetic field at which the thermal electrons are not in resonance with the EC wave. The energetic electron tail density is enhanced and a consequent increase in electron temperature and CD is observed. Up to 60–70% of EC power is estimated to be absorbed in this process. Two distinct regimes have been investigated in the FTU. In the so-called down-shifted regime the operating magnetic field is above the resonant value for EC absorption ($B = 5$ T), everywhere in the plasma. The EC waves (O-mode, outer perpendicular launch) cannot interact with the bulk electrons, whereas they can be absorbed by the suprathermal electrons tail induced by LHCD, because the relativistic mass down-shifts the cyclotron frequency. In the up-shifted regime, the operating magnetic field is below the resonant value. The EC wave is launched with an angle of 30° with respect to the magnetic field ($n_{||{\rm EC}} = 0.5$). The wave can be absorbed in the high field side of the discharge but, before thermal absorption takes place, the wave is damped on

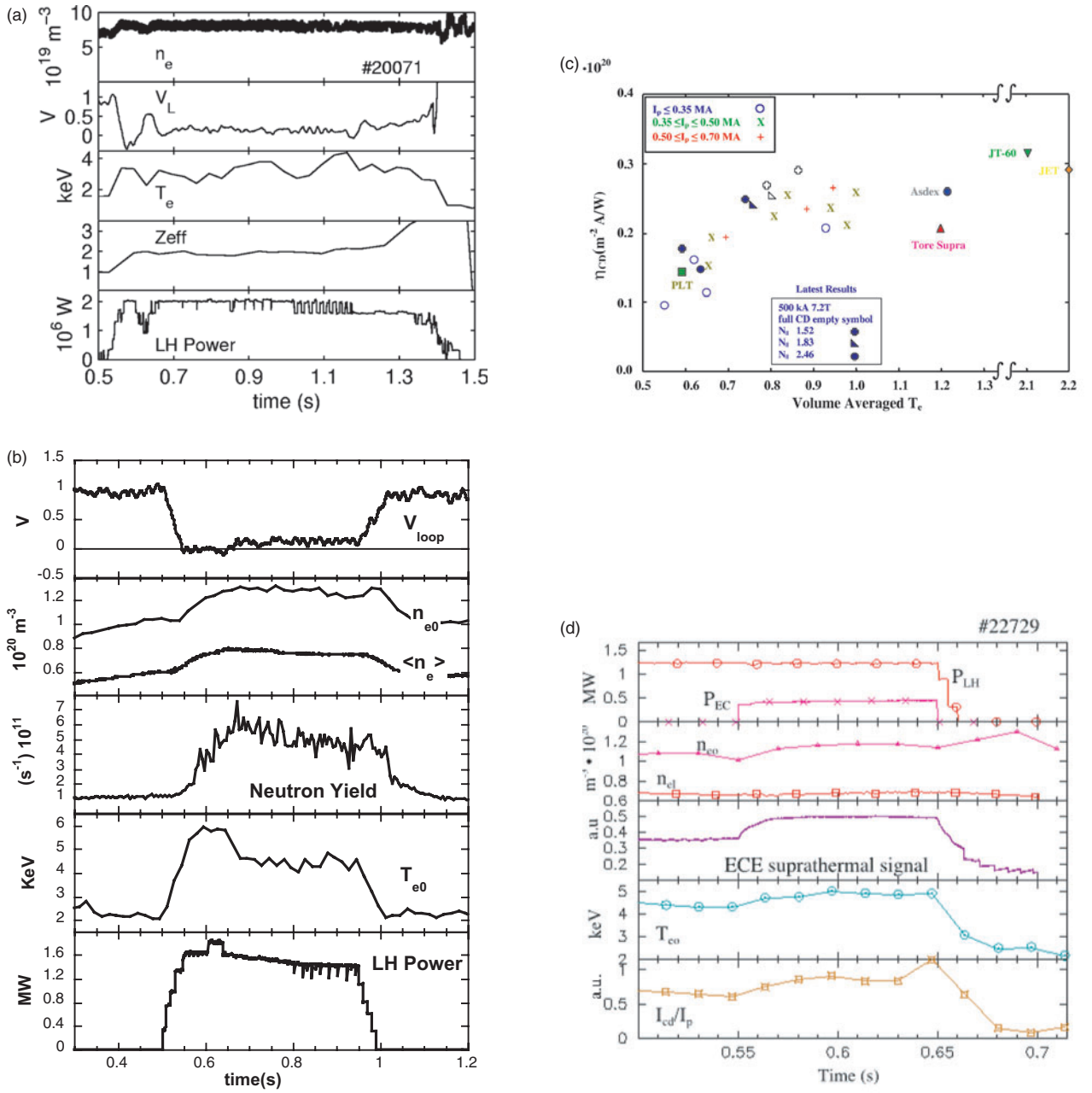

Figure 3. (*a*) Time evolution of line average (n_e) density, loop voltage (V_L), central electron temperature (T_e), Z_{eff} and LH power for a LHCD discharge at full power. Up to 2 MW for 0.8 s have been injected at ITER-relevant densities. (*b*) Time evolution of loop voltage (V_{loop}), central (n_{e0}) and line average ($\langle n_e \rangle$) density, neutron yield, central electron temperature (T_{e0}) and LH power for a LHCD discharge at ITER-relevant densities. The increase in the neutron yield indicates an increase in the ion temperature due to the electron–ion coupling at these densities. (*c*) LHCD efficiency (corrected for the Z_{eff} dependence) vs volume average electron temperature for different plasma current and magnetic field values. The values obtained in other devices are also shown. (*d*) Time behaviour of main plasma quantity in the case of down-shifted EC absorption experiment (shot #22729) at 7.2 T/0.5 MA (EC bulk resonance (5 T) outside the plasma), $Z_{eff} \approx 3$ and full LHCD.

the fast electron population. The first scheme allows a wider heating flexibility on FTU. The second scheme is of direct relevance for ITER.

The down-shifted scheme is very reproducible. The evolution of the main plasma quantities in the case of the down-shifted EC absorption experiment at 7.2 T/0.5 MA is shown in figure 3(*d*). The EC wave is injected in the perpendicular direction (with respect to the magnetic field) and the LH launched $n_{||}$ spectrum is peaked at $n_{||} = 1.82$. A clear increase of the central temperature and of the fraction of the driven current is observed. The behaviour of ECE signal evidences the increase of the suprathermal population, as expected by theory. The overall EC absorption, estimated from the residual radiation in the chamber, is 80%. Note that full non-inductive CD was achieved in this condition.

The case of up-shifted EC absorption has been performed at 5.2 T/0.6 MA. The 700 kW of launched EC leads to stabilization of the MHD activity: a clear indication of a

modification of the current profile. The current driven fraction is increased, during the EC phase, by about 50 kA, more than a factor 5 larger than the value expected from thermal absorption (8 kA) and a factor 2.5 larger than the prediction of a simplified model [12] of the suprathermal interaction (20 kA). The suprathermal EC absorption cannot be measured due to the presence of the thermal resonance in the plasma, the calculated theoretical data is 15%. The average $n_{||}$ value of the launched LH spectrum is $n_{||} = 1.82$. The impurity content corresponds to $Z_{\rm eff} = 2.7$ in the Ohmic phase with $Z_{\rm eff}$ increasing up to 6.7 during the RF injection. The up-shifted scheme will be studied in detail when the new fast electron bremsstrahlung emission cameras will allow a good determination of the fast electron density, which was not available in the 2000/2002 campaign.

4. Transport studies

4.1. Global energy confinement

Over the last five years different confinement regimes, ranging from Ohmic and L-mode plasmas to PEP and ITB plasmas, were investigated in the FTU. Transport analysis has been performed using EVITA[1] and JETTO [5] codes, yielding similar results. The database contains 20 recent FTU discharges with typical plasma parameters in the range: $B = 5.2$–7.2 T, $I = 0.35$–1.2 MA, $n_{\rm e}(0) = (0.5$–$7.3) \times 10^{20}$ m^{-3}. Some discharges contribute with more points to the database, each point corresponding to a different heating scheme (e.g. LH or LH + ECRH): the typical heating power is $P_{\rm LH} = 1.5$–2.1 MW and $P_{\rm EC} = 0.4$–0.7 MW. A summary of the FTU results on the global energy confinement is shown in figure 4(*a*). The Ohmic and L-mode discharges are generally in agreement with the ITER97 L-mode scaling. Discharges with an ITB have an energy confinement time up to 1.6 time the ITER97 scaling. The pellet discharges exhibit a time averaged confinement slightly above the ITER97 scaling, whereas gas fuelled discharges exhibit a confinement lower than the ITER97 scaling. Transient phases with enhancement factors up to 1.3 are observed but with the enhanced phase lasting less than one $\tau_{\rm E}$.

4.2. Stiffness

The FTU offers the opportunity of testing transport theories based on critical gradients at collisionality values not achievable in other tokamaks. The electron temperature profile response to strong ECRH in the FTU tokamak shows all the relevant features of stiffness: in spite of the wide range of different heating schemes (total heating power, difference in the deposition profile between Ohmic and auxiliary heated discharges), the temperature gradient length value in the confinement region (outside the sawtooth inversion radius) remains in a narrow range around $1/L_{\rm T} = 10\,{\rm m}^{-1}$ (figure 4(*b*)) [13, 14]. In the last two years, modulated ECH was used to investigate temperature stiffness using transient transport techniques. In this context, similarly to what is done for the heat pulse propagation analysis, it is convenient to define a transient value $\chi_{\rm e,HP} = \partial q_{\rm e}/\partial(n_{\rm e}\partial_{\rm r}T_{\rm e})$ (with $q_{\rm e}$ the electron heat flux) to be distinguished from the value determined from the power balance analysis. The analysis of the amplitude and phase of the induced temperature modulation has been made using a model for $\chi_{\rm e,HP}$ made by a superposition of step functions. The results are shown in figure 4(*c*). The $\chi_{\rm e,HP}$ profile is characterized by a double-step structure with the intermediate step corresponding to the edge of the region where stiffness is observed. Note that if no reduction in $\chi_{\rm e,HP}$ at $r = 8$ cm is assumed, the simulated temperature modulation amplitude does not agree with the measurements.

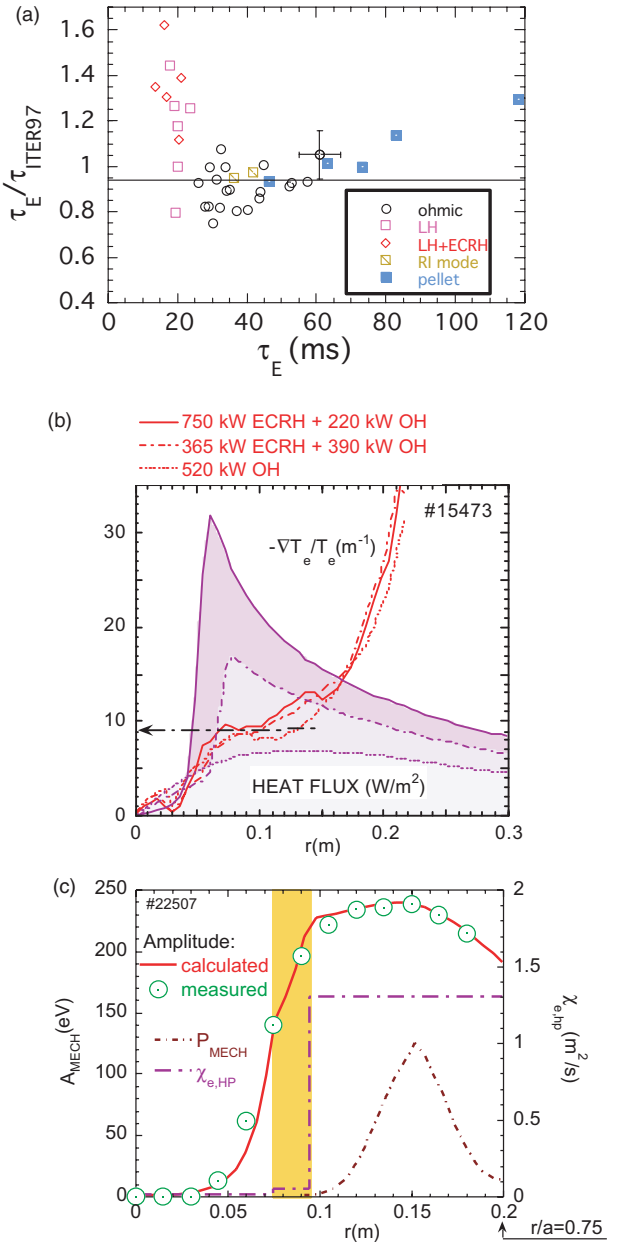

Figure 4. (*a*) Ratio of $\tau_{\rm E}$ (energy confinement time as calculated from transport analysis) to $\tau_{\rm ITER\ 97\text{-}th}$ vs $\tau_{\rm E}$. The horizontal line shows the best fit of the Ohmic data. A typical error bar is also indicated. (*b*) Temperature gradient length vs radius for the discharge #15473 during the Ohmic and auxiliary heated phase. The heat flux vs radius is also shown. (*c*) Amplitude of the temperature modulation during modulated ECH vs radius. The deposition profile and the electron thermal conductivity are also shown.

[1] http://efrw01.frascati.enea.it/Software/Unix/FTUcodici/evita/

This indicates that an electron temperature gradient driven turbulent transport with a critical value for $1/L_T$ acts also in Ohmic conditions. It is important to stress that these results apply to regions where finite magnetic shear is produced. At low magnetic shear, as, e.g. during a current ramp, no stiffness of the temperature profile has been observed in the FTU [2].

5. High density regimes

Confinement improvement by density peaking is a well-known result of several tokamaks with a possible explanation associated with ion temperature gradient mode stabilization. However, to obtain steady or quasi-steady confinement improvement with simultaneous deep fuelling is not an easy task. At the last IAEA Conference, the achievement of a quasi-steady-state enhanced confinement regime with deep pellet fuelling was reported on FTU, obtained using a multiple (eight barrel) pellet injector with a maximum speed of $1.6\,\mathrm{km\,s^{-1}}$ [15]. The density profile following the pellet injection was very peaked with central density values reaching $8 \times 10^{20}\,\mathrm{m^{-3}}$. During the last two years an effort has been made to optimize this regime and to understand the conditions to maintain such an improvement in steady-state. The interest of this regime is related to the possibility of testing the scaling at high density, high plasma current ($I \approx 1\,\mathrm{MA}$), low Z_{eff}, peaked density profiles and edge safety factor around $q_a \approx 3.3$.

In order to optimize the performance it is crucial to achieve control of the sawtooth activity as shown in figure 5 where the time evolution of two discharges is displayed. If sawteeth are suppressed after pellet injection (as in the shot #12744), heavy impurity accumulation in the centre is observed with

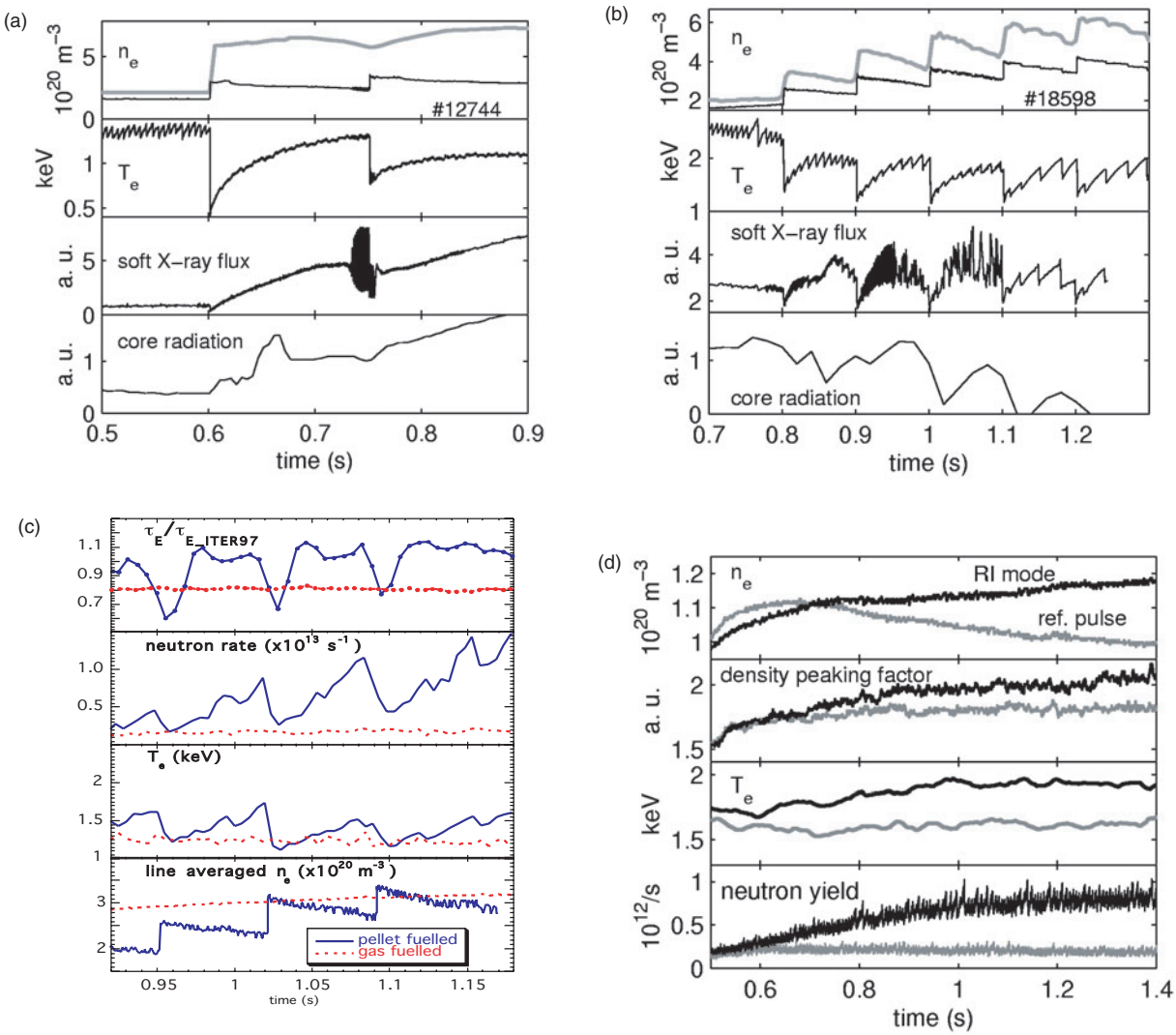

Figure 5. (*a*) Time traces for the shot #12744. After the second pellet, sawteeth are suppressed and the core radiation increases due to heavy impurity accumulation. In the first frame the grey line is the central density whereas the black line is the line average density. (*b*) Time traces for shot #18598. In this case sawteeth are delayed but not suppressed and a quasi-steady-state is achieved. In the first frame the grey line is the central density whereas the black line is the line average density. (*c*) Time evolution of the energy confinement time normalized to the ITER97 scaling, neutron rate, electron temperature and density for a gas fuelled and a pellet fuelled discharge. (*d*) Time evolution of line average density, density peaking factor, central electron temperature and neutron yield for a discharge exhibiting RI mode behaviour (black) and a reference Ohmic discharge (grey).

a substantial increase of the radiated power leading to a disruption (figure 5(*a*)). The best condition is obtained when delayed sawteeth are produced (as in shot #18598). In the FTU case, this result is achieved by a careful programming of the pellet injection time and by controlling the initial impurity content. In this case impurity accumulation is avoided and the duration of the enhanced confinement phase is limited only by the number of available pellets. Note that the impurity accumulation observed in shot #12744 requires a modification of the impurity transport coefficients with respect to the pre-pellet phase, whereas in shot #18598 the average effect of sawteeth maintains the impurity transport basically unchanged. It is apparent from these results that this enhanced confinement regime may be relevant for burning plasma operation provided sawteeth are not completely suppressed. Sawtooth control may be obtained, e.g. using RF heating.

Very high central fuelling efficiency is also observed in these discharges. The pellet ablation occurs close to the $q = 1$ surface but in a very short time particles drift towards the centre, possibly due to its closeness to the $q = 1$ surface, resulting in a peaked profile.

The power balance analysis has been performed with both JETTO and EVITA codes with similar result. Experimental data are used for the physical quantities except for the ions that are simulated with a neoclassical diffusion coefficient times an anomaly factor adjusted in order to fit the neutron yield. The Ohmic pre-pellet phase requires an anomaly factor of about 3 which reduces to 1 after the first pellet in #12744 (0.6 s) and after the third (1.0 s) in #18598. Neoclassical resistivity is always assumed, which combined with $Z_{\rm eff}$ deduced from bremmstrahlung emission, reproduces the measured loop voltage. These discharges exhibit a confinement larger than the value before pellet injection and, when a time average is performed, generally in agreement with the ITER97 L-mode scaling within the error bars. Transient confinement enhancement is observed but the duration of such a phase is less than one energy confinement time (figure 5(*c*)). The maximum confinement enhancement so far observed is a factor 1.3 times the ITER97 scaling.

RI modes have been also produced for the first time in the FTU. The FTU can extend this regime of operation to high density and high magnetic field. A comparison between an RI mode shot and a reference Ohmic shot is shown in figure 5(*d*). This 6 T/0.9 MA discharge exhibits the typical saturated Ohmic confinement behaviour. With the Ne pulse a significant increase in both the energy confinement time and the neutron yield is observed. The radiated fraction reaches a value of 90% compared to 65% before the Ne pulse. Presently, the density range was limited by the number of operating gas valves.

6. MHD studies

6.1. Internal kink mode behaviour with pellet injection

As a result of deep pellet injection, macroscopic structures with dominant $m = 1$ poloidal mode number were observed to saturate at large amplitudes and to survive across sawtooth collapses for times exceeding the resistive diffusion period (figure 6(*a*)). These structures were recognized as $m = 1$ magnetic islands with a very strong soft-x-ray emission from the O-point region as shown in figure 6(*a*). The non-linear stability of these islands seems to be due to radiative cooling around the O-point. In some cases the sawtooth activity disappears, and the $m = 2$ sideband of the $m = 1$ island develops an island at the $q = 2$ radius. In these cases the mode frequency decreases or even locks, due to the fact that flux penetration across the $q = 2$ radius gives rise to effective wall braking [16].

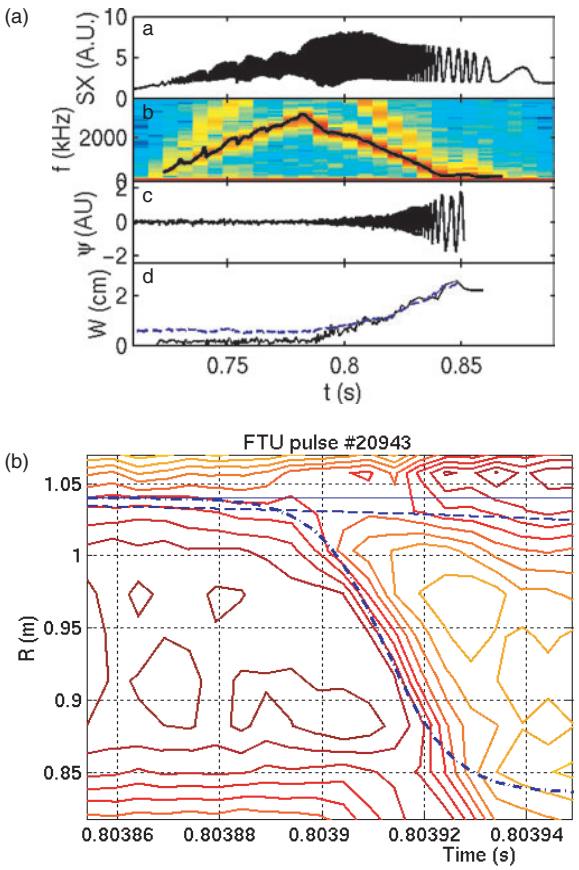

Figure 6. (*a*) Formation and evolution of an $m = 1$ structure after pellet injection at $t = 0.7$ s: (a) soft-x-ray oscillations from impurity accumulation at the island O-point; (b) spectrogram of this oscillation; (c) edge poloidal field oscillations; (d) island width evolution from ECE (black) and from magnetic coil (blue). (*b*) Temperature contours from ECE during the fast phase of a main sawtooth collapse. The island O-point is located at $R = 1.05$ m.

6.2. Reconnection studies

Careful analysis of sawtooth collapses without oscillating precursors in the FTU high density, high current plasmas revealed that the fast collapse is preceded by a purely growing $m = 1$ precursor (i.e. with zero real part of the frequency). The precursor growth rate is similar to that of the $m = 1$ mode in the semicollisional regime. At the end of the precursor phase the growth rate increases by an order of magnitude, and a final steady-state condition is reached in about 15 μs (the typical duration of purely growing and oscillating precursors are 100 μs and 1 ms, respectively). Both in the precursor and in the fast collapse phase the plasma core structure is consistent with the one assumed in the Kadomtsev model, i.e.

the central region undergoes a top-hat displacement leaving room to a crescent-shaped $m = 1$ island. The final (relaxed) configuration can be partly or almost fully reconnected; two (nearly) full reconnection events are typically interleaved by one or two partial reconnection events. In partial reconnection the displacement saturates at a value that is typically below 50% of the $q = 1$ radius; in these cases decaying post-cursor oscillations are observed.

In figure 6(*b*) the evolution of temperature contours (representative of the magnetic surfaces) is shown during the fast collapse phase for a (nearly) full reconnection case. The solid line in figure 6(*b*) shows the position of a magnetic surface near the inversion radius before the precursor appearance. In the early phase of the collapse evolution, the displacement of such a surface follows an exponential growth (dashed curve in figure 6(*b*)) with a growth rate in agreement with the theoretical estimate in the semicollisional regime [17]. The displacement velocity, as evaluated from the slope of temperature contours, dramatically increases at $t = 0.8039$ s and then saturates. The dot-dashed line is obtained from a non-linear model assuming a constant reconnection rate, about 10 times larger than the linear growth rate [17]. The final displacement is at least 80% of the sawtooth inversion radius, but reconnection is not properly full as a tiny $m = 1$ structure survives.

7. Future plans

The FTU will resume operation at the beginning of 2003. The main objective of the 2003 campaign will be the testing and characterization of the passive active module envisaged as the LH launching structure for ITER. In the second half of 2003 the new scanning CO_2 interferometer and the motional Stark effect diagnostics will be inserted. Experiments will be performed on vertical pellet injection.

The analysis of possible enhancements of FTU has continued. The possibility of a substantial upgrade of FTU in a D-shaped device (FT3) operating up to 8 T, 6 MA has been investigated. The device equipped with the same diagnostic and auxiliary heating systems of FTU, with the addition of 20 MW ICRH power at 70–90 MHz, could be inserted in the FTU hall and would make full use of the Frascati site credits. The main scientific aim would be the investigation of collective effects in burning plasmas, by simulating the alpha particle behaviour with the fast ion produced by intense ICRH, and the preparation of ITER scenarios. Thanks to the short construction period (five years) this device could be a JET-class tokamak (capable of achieving equivalent fusion gain between $Q = 1$ and 5) for the accompanying programme during the ITER construction period.

References

[1] Cirant S. *et al* 1997 *Proc. 10th Joint Workshop on ECE and ECRH* ed T. Donne and Toon Verhoeven, p 369

[2] Buratti P. *et al* 1999 High core electron confinement regimes in FTU plasmas with low or reversed magnetic shear and high power density electron cyclotron resonance heating *Phys. Rev. Lett.* **82** 560

[3] Barbato E. 2001 ECRH studies: internal transport barriers and MHD stabilisation *Plasma Phys. Control. Fusion* **43** A287

[4] Castaldo C. *et al* 2002 Electron internal transport barriers with ECRH and LHCD in the FTU tokamak *Proc. 29th EPS Conf. on Control. Fusion and Plasma Phys. (Montreux, 17–21 June 2002)*

[5] Cenacchi G. and Taroni A. 1988 JETTO: a free boundary plasma transport code *ENEA Report* RT/TIB/88/5

[6] Tresset G. *et al* 2002 *Nucl. Fusion* **42** 520

[7] Cesario R. *et al* 2001 Reduction of the electron thermal conductivity produced by ion Bernstein waves on the Frascati Tokamak Upgrade tokamak *Phys. Plasmas* **8** 4721

[8] Podda S. *et al* 2002 Lower hybrid current drive and heating experiments at high density in the FTU tokamak *Proc. 3rd IAEA Technical Committe Meeting on Steady-State Operation of Magnetic Fusion Device (Arles, France, 6–7 May 2002)*

[9] Pericoli-Ridolfini V. *et al* 2002 Progress towards internal transport barriers at high plasma density sustained by pure electron heating and current drive in the FTU tokamak *Paper* EX/C3-6, FEC 2002 (Lyon)

[10] Pericoli V. *et al* 1999 High plasma density lower hybrid current drive in the FTU tokamak *Phys. Rev. Lett.* **82** 93

[11] Granucci G. *et al* 2001 Combined LH and ECRH waves injection in FTU tokamak *Proc. 28th EPS Conf. on Control. Fusion and Plasma Phys. (Funchal, Portugal, 18–22 June 2001)*

[12] Farina D. and Pozzoli R. 1989 *Phys. Fluids* B **1** 1042–8

[13] Sozzi C. *et al* 2000 *Proc. 18th Int. Conf. on Fusion Energy 2000 (Sorrento, 2000)* (Vienna: IAEA) CD-ROM file EXP5/13 and http://www.iaea.org/programmes/ripc/physics/fec2000/html/node1.htm

[14] Cirant S. *et al* 2002 Experiments on electron temperature profile resilience in FTU tokamak with continuous and modulated ECRH *Proc. 19th Int. Conf. on Fusion Energy 2002 (Lyon, 2002)* (Vienna: IAEA) CD-ROM file EX/C4-2Rb and http://www.iaea.org/programmes/ripc/physics/fec2002/html/fec2002.htm

[15] Frigione D. *et al* 2001 Steady improved confinement in FTU high field plasmas sustained by deep pellet injection *Nucl. Fusion* **41** 1613

[16] Giovannozzi E. *et al* 2002 Island structure and rotation after pellet injection in FTU *Proc. 19th Int. Conf. on Fusion Energy 2002 (Lyon, 2002)* (Vienna: IAEA) CD-ROM file EX/P4-11 and http://www.iaea.org/programmes/ripc/physics/fec2002/html/fec2002.htm

[17] Buratti P., Giovannozzi E. and Tudisco O. 2003 Purely growing precursors and sawtooth trigger mechanisms *Plasma Phys. Control. Fusion* **45** L9